Charge in Long-Lasting El Niño Events by Convection-Induced Wind Anomalies over the Western Pacific in Boreal Spring

ZHENNING LI

School of Atmospheric Sciences, Sun Yat-sen University, Guangzhou, China

SONG YANG

School of Atmospheric Sciences, and Guangdong Province Key Laboratory for Climate Change and Natural Disaster Studies, and Institute of Earth Climate and Environment System, Sun Yat-sen University, Guangzhou, China

XIAOMING HU

School of Atmospheric Sciences, and Guangdong Province Key Laboratory for Climate Change and Natural Disaster Studies, Sun Yat-sen University, Guangzhou, China

WENJIE DONG

School of Atmospheric Sciences, and Guangdong, Hong Kong and Macao Joint Laboratory for Tropical Oceanic-Atmospheric System Science, Sun Yat-sen University, Guangzhou, China

BIAN HE

State Key Laboratory of Numerical Modeling for Atmospheric Sciences and Geophysical Fluid Dynamics, Institute of Atmospheric Physics, Chinese Academy of Sciences, Beijing, China

(Manuscript received 17 August 2017, in final form 11 February 2018)

ABSTRACT

In this study, El Niño events are classified as long El Niño (LE) events and short El Niño (SE) events based on their durations, and the characteristics of the early stages of these events are investigated. Results indicate that LE events tend to start earlier compared to SE events, initiating in boreal spring and peaking in winter. Their early occurrence is attributed to the western equatorial Pacific (WEP) sea surface wind anomalies that benefit the eastward propagation of warm water by forcing the downwelling Kelvin waves. It is also found that the wind anomalies are potentially induced by the convection anomalies over the WEP in spring. Experiments with a fully coupled climate model forced by convection heating anomalies over the WEP show that El Niño events become stronger and longer after introducing anomalous convection heating. The convection anomalies induce an extensive anomalous westerly belt over the WEP, which charges El Niño by eastward-propagating Kelvin waves. Moreover, induced by the anomalously northward-shifted ITCZ heating and the suppressed heating over the Maritime Continent, the equatorially asymmetric westerly belt reduces the meridional shear of mean easterly wind in the lower latitudes, which maintains an anomalous equatorward Sverdrup transport and in turn prolongs the persistence of El Niño events. A case study of the 2015/16 super El Niño and a regression study by using a rainfall index in critical regions support the above results.

1. Introduction

Predicting the occurrence, duration, and strength of potential El Niño events realistically provides the most critical skill for interannual climate prediction (Latif et al. 1998; Morss and Battisti 2004; Kumar et al. 2015). Since El Niño–Southern Oscillation (ENSO) was recognized as a coupled ocean–atmosphere phenomenon, Cane et al. (1986) developed a simple model capable of predicting El Niño events up to nine months in advance.

Denotes content that is immediately available upon publication as open access.

Supplemental information related to this paper is available at the Journals Online website: https://doi.org/10.1175/JCLI-D-17-0558.s1.

Corresponding author: Dr. Song Yang, yangsong3@mail.sysu.edu.cn

DOI: 10.1175/JCLI-D-17-0558.1

However, many models based on Cane et al. (1986) suffer from rapid decrease in forecast skill in the boreal spring, namely the spring predictability barrier (SPB; Webster and Yang 1992). Associated with the seasonal phase-locking feature of ENSO, the SPB has been attributed to the weakest near-equatorial circulation and ENSO variation in springtime (Webster and Yang 1992; Torrence and Webster 1998). Meanwhile, Webster and Yang (1992) and Lau and Yang (1996) suggested that the rapidly developing strong Asian monsoon helps to ''bridge'' the barrier in spring.

To test the hypothesis, Webster (1995) demonstrated that the duration of an El Niño event was altered substantially by intensifying the monsoon system in a coupled model, possibly because of the coherent alterations of wind stress in the Pacific Ocean. Xu and Chan (2001) pointed out that the anomalous convergence of the Asian winter monsoon northerlies and the southerlies associated with the transition of the Australian monsoon could strengthen the westerly anomalies over the western equatorial Pacific (WEP), triggering an ensuing El Niño event. Later, regional decoupled experiments, which represent prescribing SST in a certain ocean in a fully coupled model, showed that the Indian Ocean variability (associated with the Asian monsoon variability) contributed to the biennial ENSO tendency (Yu et al. 2009; Terray et al. 2016). To summarize, the monsoon system is likely to bridge the SPB by modulating the frequency of ENSO periodicity.

On a subseasonal time scale, as potential triggers for El Niño events, westerly wind events (WWEs) over the WEP have been drawing attentions for decades (Harrison and Vecchi 1997; Lengaigne et al. 2004; Menkes et al. 2014). Recent studies suggested the WWEs were also responsible for the buildup of equatorial Pacific warm water volume (WWV) through downwelling Kelvin waves (e.g., McGregor et al. 2016). Since the WWV anomalies provided a reliable indicator for El Niño's peak SST anomalies (SSTAs) around nine months later (McPhaden 2012), the seasonal phase-locking character of El Niño events implied that boreal springtime WWEs were crucial for predicting the warm events. Hence, following the view of Webster and Yang (1992), we anticipate that springtime WWE performs as an intermediary to link monsoon development and El Niño variability.

For the rest of this article, section 2 introduces datasets and analysis methods. In section 3, a method of classifying El Niño events based on their durations is documented. Section 4 examines the relationship between different types of El Niño events and the evolutions of various parameters in boreal spring. Model response to anomalous springtime convection heating and a case study for the super El Niño event in 2015/16 are archived in section 5. The main results obtained are summarized and discussed in section 6.

2. Datasets and methods

a. Datasets

The 3-month-running mean of the Niño-3.4 SST index, which is termed the oceanic Niño index (ONI), is obtained from the National Oceanic and Atmospheric Administration/Climate Prediction Center (NOAA/CPC; http://www.cpc.ncep.noaa.gov/products/analysis_monitoring/ensostuff/ensoyears.shtml). To qualify an El Niño event by NOAA/CPC, the ONI value must be above 0.5°C for 5 consecutive months. In this study, the LE episode is defined as the warm event with an ONI value above 0.5°C for 10 consecutive months. To provide further confidence in such classification, we have also applied 9 and 11 months as the criterion for sensitivity tests and found that the robustness of the main features obtained in the study was not influenced.

The global gridded SST data are obtained from the Hadley Centre, which provides monthly mean SST and sea ice concentration in a $1° \times 1°$ spatial resolution. Two global monthly mean precipitation datasets are used: the Global Precipitation Climatology Project, version 2.2, available since 1979 (Adler et al. 2003) and the Climate Prediction Center (CPC) Merged Analysis of Precipitation (Xie and Arkin 1997). Monthly atmospheric fields are from the National Centers for Environmental Prediction (NCEP)–U.S. Department of Energy (DOE) Atmospheric Model Intercomparison Project phase II (AMIP-II) reanalysis (Kanamitsu et al. 2002). Both the precipitation data and the AMIP-II reanalysis cover the period of 1979–2016 and are gridded in a $2.5° \times 2.5°$ spatial resolution. Oceanic reanalysis (1980–2016) consisting of $0.5° \times 0.5°$ gridded variables for global oceans is obtained from the Simple Ocean Data Assimilation, version 3.3.1 (SODA3; Carton et al. 2000).

b. Model experiments

The Community Earth System Model (CESM), version 1.2.2 (Hurrell et al. 2013), is used to investigate the role of atmospheric convection heating in modulating El Niño events. A fully coupled simulation of 300 years with the B_2000 component setting implemented as the baseline simulation. Because of the model bias in simulating the phase locking behavior of ENSO onset and termination, the simulated El Niño events can initiate anytime in the model year (Neelin et al. 2000; MacMynowski and Tziperman 2008). Therefore, the

TABLE 1. Comparison between long El Niño and short El Niño events. (MJJ is May–July, ASO is August–October, JFM is January–March, AMJ is April–June, OND is October–December, and FMA is February–April.)

Years	Occurrence time	Termination time	Duration (months)	Peak SSTA (°C)
LE episodes				
1982/83 (EP)	MAM 1982	MJJ 1983	14	2.1
1986–88 (EP)	ASO 1986	JFM 1988	17	1.6
1991/92 (CP)	MJJ 1991	JJA 1992	13	1.6
1997/98 (EP)	AMJ 1997	AMJ 1998	12	2.3
2014/16 (CP)[a]	OND 2014	AMJ 2016	21	2.3
SE episodes				
1979/80 (CP)[b]	SON 1979	JFM 1980	5	0.6
1994/95 (CP)	SON 1994	FMA 1995	6	1.0
2002/03 (CP)	MJJ 2002	JFM 2003	9	1.2
2004/05 (CP)	JJA 2004	MAM 2005	10	0.7
2006/07 (EP)	ASO 2006	DJF 2007	5	0.9
2009/10 (CP)	JJA 2009	MAM 2010	10	1.3

[a] According to Lim et al. (2017).
[b] According to Wang et al. (2018).

traditional way to implement sensitive experiment at a spunup point and continue integration for several decades does not work well for interpreting the role of convective heating at the early stage of warm events. To deal with this problem, in the model integration, we impose a constant westerly forcing ($10\,m\,s^{-1}day^{-1}$) during Julian days 15–75. The forcing is set in the domain 10°S–10°N, 120°E–180°, with an *e*-folding damping from the surface to around 800 hPa (through model layers 21–26). The operation ensures that the ensemble mean evolves into a weak El Niño condition. The above operation is done in year 262 of the spunup model, and we perturb the atmospheric initial condition on 1 January to build the control (CTRL) ensemble run. In the sensitive (SEN) experiment, the only difference compared to the CTRL group is the modified convective heating in MAM (1 March–31 May). The modification is achieved through changing the convective heating term in the temperature prognostic equation in every time step. The heating rate calculated from the convection scheme is modified by 10% from 850 to 300 hPa approximately (model layers 16–23), with intensifying operation in boxes A + B and suppressing operation in box C (see Fig. 3a). A total of 25 ensemble members with initial disturbances are employed in both control and sensitive experiments.

3. Classification of El Niño events

Xu and Chan (2001) investigated the relationship between El Niño onset and Asian–Australian monsoon circulation by separating El Niño events into spring onset type and summer onset type. Since a number of studies suggested that the monsoon system was likely to modulate the duration of El Niño events (Webster 1995; Yu et al. 2009), we imitated Xu and Chan (2001) but divided El Niño events into long El Niño (LE) and short El Niño (SE) based on their durations using the ONI during 1979–2016 (see section 2 for details).

The result of classification of El Niño based on their durations is overall consistent with that based on El Niño onset time by Xu and Chan (2001), meaning that long persistent El Niño events also tend to start earlier, and vice versa. Although each El Niño event has its own characteristics, the common properties ensure the feasibility to conduct the classification (see Fig. S1 in the supplemental material for Niño-3.4 SSTA evolution in individual event). Both peak Niño-3.4 SSTA (Table 1) and composite SSTA time series (Fig. 1a) indicate that the LE type of El Niño has larger SST amplitude, with a maximum SSTA of 1.8°C. In contrast, the SE type only reaches a maximum of 1.0°C. On average, the LE type sustains the El Niño state for 11 months, while the SE type only persists for 7 months. Interestingly, the maximum anomalies of both types occur in December, implying that the mature phase of El Niño event is highly phase locked with the annual cycle. On the other hand, Fig. 1b demonstrates that the WEP (5°S–5°N, 130°–160°E) SST is dominated by a semiannual cycle, and the SST increases rapidly in spring. Therefore, the springtime warmer water in the WEP potentially exerts an influence on El Niño development if it propagates eastward by suitable external forcing. Of note is that in the recent El Niño events are indeed associated with SST and subsurface anomalies confined over the central Pacific, which are classified as central Pacific (CP) El Niño events (Kao and Yu 2009; Kug et al. 2009; Lee and McPhaden 2010; Lee et al. 2010; Yu et al. 2012). A comparison between the two categorizations is summarized in Table 1. Results indicate that most eastern

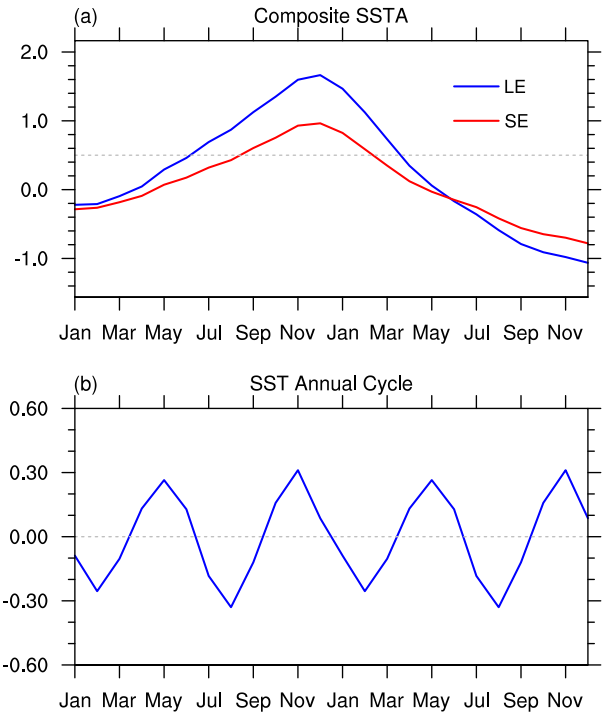

FIG. 1. (a) Composite time series of the SSTAs (K) over Niño-3.4 region for the two types of El Niño episodes. (b) Seasonal cycle of SST (K) relative to the annual mean over the WEP.

Pacific (EP)-type El Niño events belong to the LE events, and there is only one EP-type El Niño event (2006/07) in the six SE events. Therefore, the EP-type El Niño events tend to occur earlier in the annual cycle and persist longer compared to the CP-type El Niño events (Yu et al. 2010).

4. Large-scale environmental parameters related to different types of El Niño events

To test the above assumption, we first examine the March–May (MAM) climatology of various large-scale parameters. As seen in Fig. 2a, SST is above 28°C within 15°S–15°N over the western and central Pacific, with a maximum value above 30°C south of the equator. Rainfall distribution is overall in line with the SST distribution, while the maximum rainfall is over the intertropical convergence zone (ITCZ) about 5° north of the equator. As illustrated in Fig. 2b, strong sea surface northeasterly wind prevails over the northern WEP. In contrast, southeasterly wind is weak over the southern WEP. In response to the surface zonal wind distribution, the Ekman transport in the mixed layer is stronger in the Northern Hemisphere (Fig. 2c). Therefore, the divergence in the equatorial mixed layer is mainly contributed to by the Northern Hemisphere poleward Ekman current (Fig. 2c). Associated with the strong meridional shear of zonal wind near the ITCZ, the largest positive wind stress curl appears along 10°N (Fig. 2b). Thus, the shallowest thermocline forms near 10°N because of the Sverdrup balance (Fig. 2c; Lu and McCreary 1995). Moreover, zonally averaged precipitation and easterly wind speed in Fig. 2d clearly demonstrate that the climatological maxima of rainfall and wind are located over 5°N and 12°N, respectively.

Based on the above result, we then conduct a composite analysis according to different types of El Niño events. Figure 3 displays the composite differences of LE events minus SE events. Overall, the SST and rainfall anomalies over the western Pacific show early stage features of El Niño events. Specifically, cold SSTAs are found over the northern WEP and rainfall becomes reduced over the Maritime Continent (MC) and shifts eastward. These features are distinct in the LE events since the composite differences of LE events minus climatology also show similar results (see Fig. S2 in the supplemental material).

Figure 3b denotes the composite differences in sea surface wind, in which a remarkable cyclonic circulation appears over the northern WEP. Note that broad westerly anomalies prevail near the equator, which is responsible for the buildup and eastward propagation of equatorial warm water through the generation of downwelling Kelvin waves (McPhaden 2012). Furthermore, the broad westerly belt reduces the meridional shear of mean easterly wind in the lower latitudes. Therefore, the weakened wind curl maintains an anomalous equatorward Sverdrup transport, which charges the equatorial WWV and deepens the thermocline (Fig. 3c). As suggested by McGregor et al. (2016), the off-equatorial WWE is responsible for maintaining the equatorial WWV by damping the discharge effect as a result of the boundary reflections of upwelling Rossby waves. Accordingly, the features from the composite analysis are asymmetric about the equator, meaning that the off-equatorial westerly anomalies in the Northern Hemisphere may be a dominant contributor to the long-lasting El Niño events. Furthermore, rainfall anomalies peak to the north of the climatological precipitation center in the ITCZ by about 3° latitude (Fig. 3d), and a cyclonic anomaly, with broad westerlies straddling the equator east of the dryer MC, is centered over the northwest to the enhanced precipitation in the ITCZ. According to Gill (1980), the surface wind anomalies seem to be a combination of the Kelvin-plus-Rossby wave responses to the convective heating anomalies in the boxes in Fig. 3a. Thus, we raise the following hypothesis: off-equatorial westerly anomalies are induced by the anomalous convective heating over

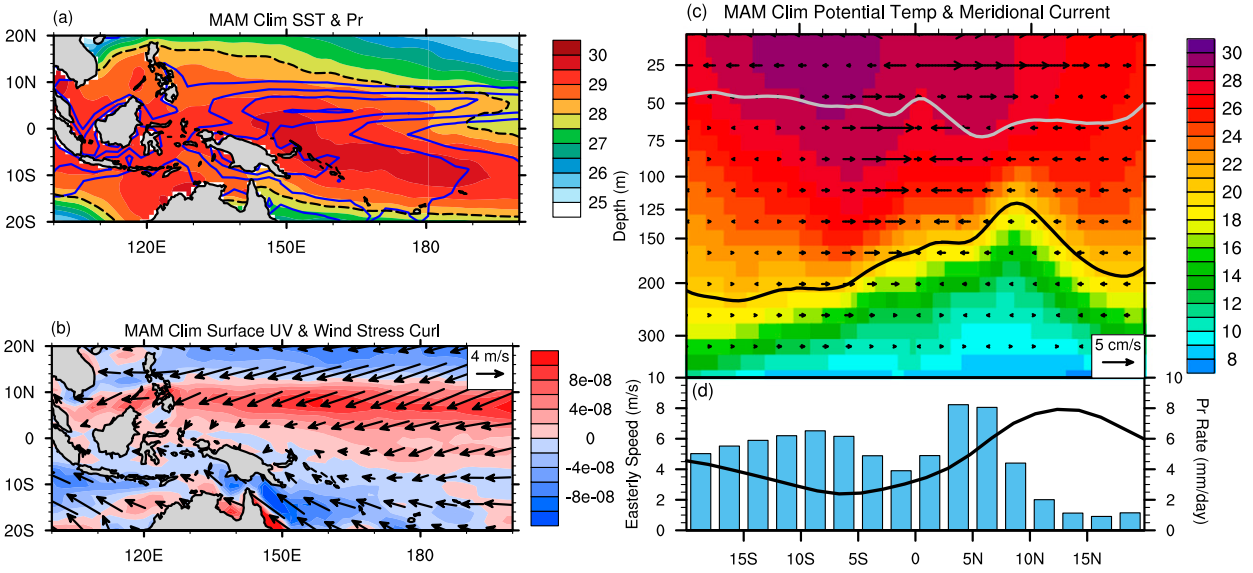

FIG. 2. (a) Shaded areas show the climatological (1979–2015) MAM SST (°C). Black dashed contours show the 28°C isotherm. Blue contours with 2.0 mm day^{-1} intervals denote the areas where the climatological precipitation exceeds 4.0 mm day^{-1} (outermost contour). (b) Shaded areas indicate the sea surface wind stress curl (Pa m^{-1}), and vectors denote the sea surface wind (m s^{-1}). (c) Shaded areas and vectors display the zonally averaged seawater potential temperature (°C) and oceanic meridional current (cm s^{-1}) over 150°E–180° [meridional range: 20°S–20°N; see (d)], respectively. Gray and black curves show the mixed layer depth [defined by temperature criterion according to de Boyer Montégut et al. (2004)] and 20°C potential temperature depth, respectively. (d) Blue bars and black curve denote the zonally averaged precipitation and easterly wind speed over 150°E–180°, respectively.

the MC and the WEP, and in turn enhance and prolong the ensuing El Niño events from their early stage.

5. Model response to anomalous springtime convective heating and signature of the 2015/16 super El Niño

We apply the CESM, version 1.2.2 (Hurrell et al. 2013), to test the above hypothesis. Because of the model bias in simulating the phase locking behavior of ENSO onset and termination, the simulated El Niño events can initiate anytime in the model year (Neelin et al. 2000; MacMynowski and Tziperman 2008). To overcome this bias, a prescribed westerly forcing is implemented to ensure the model evolves into a weak El Niño condition (see section 2). Figure 4a displays the evolution of Niño-3.4 SSTA in the CTRL and SEN runs. The ensemble mean from the CTRL implies a typical weak El Niño event that peaks with a maximum SSTA of 0.7°C in January. However, in SEN, SST rises much faster when the heating modification in MAM is switched on and peaks at 1.4°C in boreal winter. After the peak, the El Niño condition demises rapidly in the ensuing year, returning to the similar state compared to CTRL.

The above results support the hypothesis that the anomalous convective heating over the MC and the WEP can change El Niño evolutions. How does the atmospheric circulation change in the associated processes? Figures 4b,c depict the composite differences in spring precipitation, surface wind, and wind curl between SEN and CTRL. The change in rainfall is overall consistent with the observed, with more northeastward-shifted ITCZ and dryer MC (Fig. 4b), but there is no significant change in the southern WEP. Meanwhile, a strong and extensive anomalous westerly belt appears in the WEP and peaks at 5°N (Fig. 4c). Although the surface cyclonic response is not apparent over the northern WEP, a center of surface wind convergence is found near 10°N, 160°E (Fig. 4b). Note that although the magnitude is weaker, the pattern of surface wind curl mimics that in the observation, which is important for maintaining an anomalous equatorward Sverdrup transport.

We further investigate the 2015/16 super El Niño as a case analysis to test the potential role of convective anomalies based on the above results. In early 2014, people wondered whether the potential following El Niño would rival the catastrophic 1997/98 warm event based on certain early indicators (e.g., Tollefson 2014). However, most predictions flopped and the strong warm event became a latecomer in 2015 (Fig. 5a). The differences in precipitation and surface wind between the 2015 MAM mean and the 2014 MAM mean (former

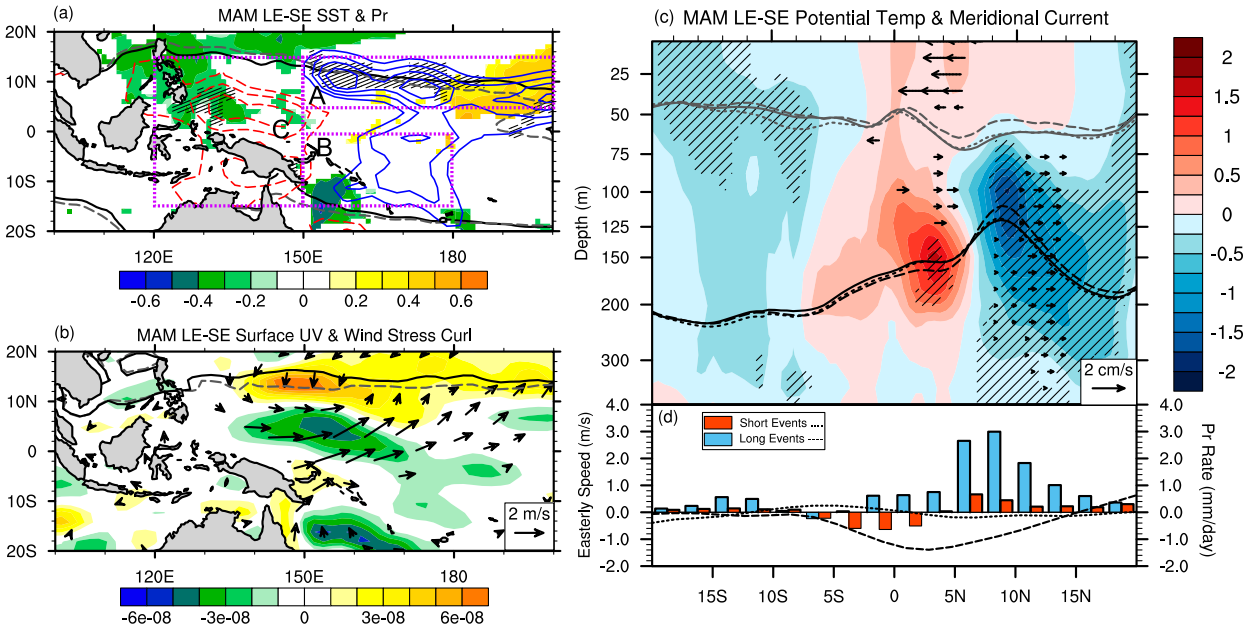

FIG. 3. Composite results of LE events minus SE events in the developing spring (MAM). (a) Color shading indicates SST differences (K) between long events and short events with areas of <90% confidence level masked out. Solid blue (dashed red) contours at 0.5 mm day^{-1} intervals denote the areas where precipitation differences exceed 1.0 (−1.0) mm day^{-1} with values above the 90% confidence level marked by black hatching. Black solid contours and gray dashed contours demonstrate the 28°C isotherms for long cases and climatology, respectively. (b) Shaded areas show the differences in wind stress curl (Pa m^{-1}) and vectors denote the differences in surface wind. Black solid contours and gray dashed contours demonstrate the locations of zero wind stress curl north of 5°N for long cases and climatology, respectively. (c) Shaded areas display the differences in zonally averaged (20°S–20°N, 150°E–180°) seawater potential temperature (K) in which values above the 90% confidence level are marked by black hatching. Vectors show the differences in zonally averaged oceanic meridional current (values below the 90% confidence level are masked out). Gray solid, dashed, and dotted curves denote the mixed layer depth for climatology, long events, and short events, respectively. Black curves are the same as gray curves but for the 20°C potential temperature depth. (d) Blue and red bars display the zonally averaged precipitation departures between long events and climatology, and between short events and climatology, respectively. Dashed and dotted curves show the easterly wind speed departures for long events and short events, respectively.

minus latter) show remarkable resemblance between Figs. 5b and 4b, which means that the convection–wind coupling pattern only exists in the onset year. The prominent westerly wind over the WEP could play a key role in triggering a super El Niño in 2015 by downwelling Kelvin waves. However, the difference in surface wind curl was insignificant (Fig. 5b), indicating that curl-driven poleward transport might not be a contributor for the failure of 2014 El Niño forecast. To obtain a potential forecasting index, we analyze the relationship between the Niño-3.4 domain-averaged DJF SSTA and the MAM precipitation index calculated by $I = (A + B)/2 - C$ with respect to the domain-averaged precipitation in the boxes of A through C in Fig. 3a (see Fig. 5c). The coefficient of correlation between the SSTA and precipitation indices is 0.61, which proves that the spring rainfall anomaly pattern is an indicator for the state of following wintertime ENSO events. In addition, the relationship is even tenable in the opposite La Niña phase.

6. Summary and discussion

In this study, two types of El Niño events are classified based on their durations. Results indicate that the earlier occurrence, longer persistence, and stronger peak of LE events are attributed to the WEP sea surface wind anomalies, which are induced by the convective anomalies over the MC and the WEP in spring. Both observational and model results show that the extensive westerly belt induced by convective heating anomalies is responsible for charging potential El Niño events by two mechanisms. First, the extensive anomalous westerly belt benefits an eastward propagation of warm water by forcing the oceanic Kelvin waves in spring. Second, induced by the enhanced convective heating associated with anomalously northward-shifted ITCZ and the suppressed heating over the MC, the equatorially asymmetric westerly belt reduces the meridional shear of mean easterly wind in the lower latitudes in the WEP. Therefore, the weakened wind curl maintains an anomalous equatorward Sverdrup transport, which

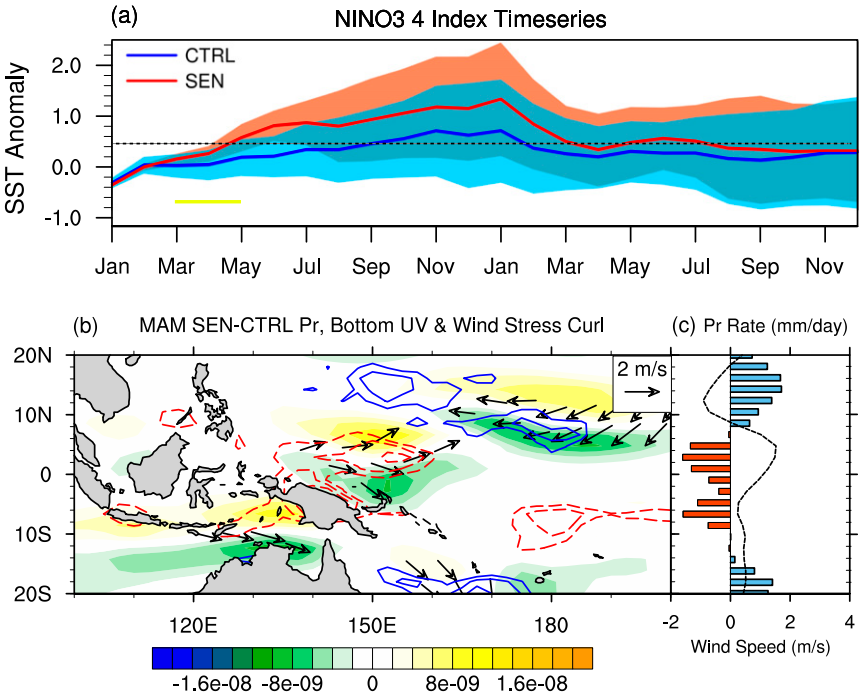

FIG. 4. (a) ONI (K) for ensemble members of 25 CESM CTRL runs (blue curves) and ensemble members of 25 SEN runs (red curves). Thick blue (CTRL) and red (SEN) curves are for the ensemble means, and light blue (CTRL) and red (SEN) shading is for the range of one standard deviation, respectively. The yellow bar from March to May demonstrates the convection heating modification periods. (b) Shaded areas show the differences in wind stress curl (Pa m^{-1}) between the SEN ensemble mean and the CTRL ensemble mean, and vectors denote the differences in surface wind (values of wind speed smaller than 1.0 m s^{-1} are masked out). Solid blue (dashed red) contours at 0.5 mm day^{-1} intervals denote the areas where precipitation differences exceed 1.5 (−1.5) mm day^{-1} (outermost contours). (c) Differences in zonally averaged precipitation (bars) and westerly wind speed (curve) between the SEN ensemble mean and the CTRL ensemble mean over 20°S–20°N, 140°E–180°.

charges the equatorial WWV and deepens the thermocline. Both a case study of the super El Niño event in 2015/16 and a regression study using an index defined as convective heating anomalies in critical regions support the hypothesis. Therefore, the springtime convection anomalies over the WEP may help to "bridge" the SPB.

Results of this study appear to have provided an emphasis on the role of the convection anomaly in charging El Niño events at their early stage. However, several questions still remain to be answered. First, the regions with anomalous convection are generally over oceans and it is difficult to be linked directly to the initial motivation: monsoon variability. Nevertheless, the drying trend over the MC and the northward shift of the ITCZ may reflect a rapid seasonal transition from winter to summer (Chang et al. 2005). Following Xu and Chan (2001), recent studies also emphasized the contribution of the anomalous Asian–Australian monsoon convergence to the surface westerlies over the WEP preceding El Niño onset (e.g., Zheng et al. 2014). Second, results from the current study are based on seasonal means, which is unable to reveal the driver of convection anomaly. On a subseasonal time scale, previous studies have shown that the Madden–Julian oscillation or even extratropical forcing may trigger El Niño events by expanding zonal range of westerly forcing and generating stronger Kelvin waves (e.g., Bergman et al. 2001; Zhang 2005; Hong et al. 2017). Also, evidence exists that the positive Indian Ocean dipole (IOD) can generate cross-basin wind anomalies that modify the Pacific ENSO evolution (Saji and Yamagata 2003; Kug and Kang 2006; Cai et al. 2011). However, the drying of MC and the extension of warm pool convection are also important responses to El Niño signals. Therefore, at the early stage of El Niño events, if convection distribution and related surface wind response over the WEP mimic the

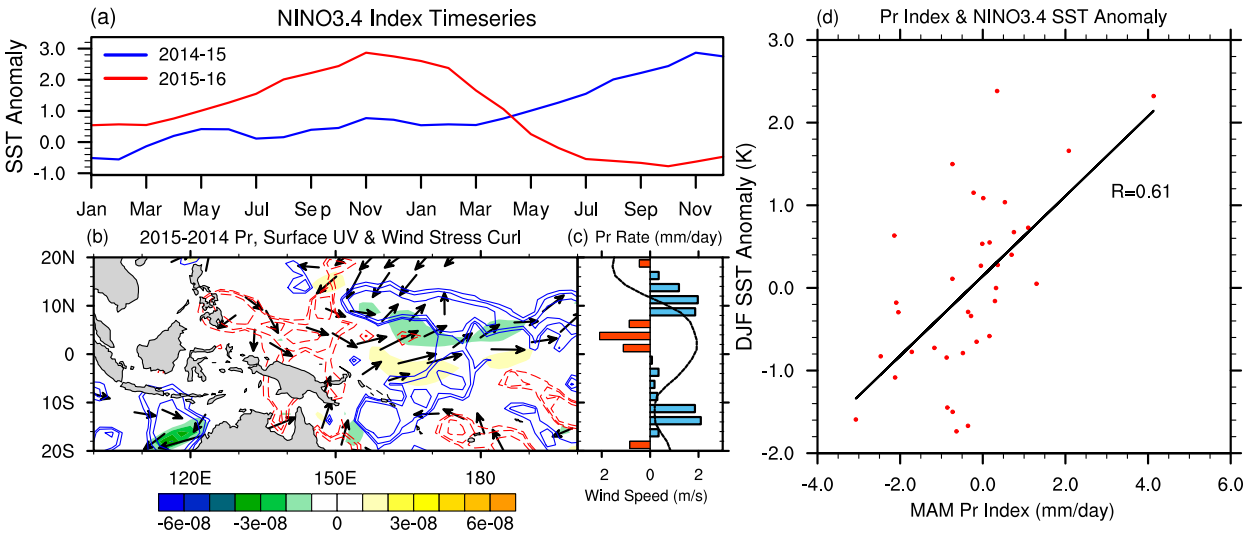

FIG. 5. (a) ONI time series (K) for 2014/15 (blue curve) and 2015/16 (red curve). (b),(c) As in Fig. 4b,c, but for 2015 MAM mean minus 2014 MAM mean. (d) Scatterplot for the relationship between Niño-3.4 domain-averaged DJF SSTA (K) and the MAM precipitation index (mm day^{-1}) calculated by formula (A + B)/2 − C with respect to the domain-averaged precipitation in the boxes shown in Fig. 3a.

results presented in this study, a self-sustained mechanism may exist to strengthen and prolong the warm events by intensifying the strength of air–sea coupling (Cai 2003).

Acknowledgments. The authors thank Prof. John Chiang of the University of California at Berkeley and the three anonymous reviewers who provided helpful comments and suggestions for improving the overall quality of the paper. This study was supported by the National Key Research Program of China (Grant 2014CB953904), the National Natural Science Foundation of China (Grants 41690123 and 41690120), the "111-Plan" Project of China (Grant B17049), the Jiangsu Collaborative Innovation Center for Climate Change, and the Zhuhai Joint Innovative Center for Climate, Environment and Ecosystem. Computing resource for the CESM was provided by the high-performance grid computing platform of Sun Yat-sen University and the "Tianhe-2" in the National Supercomputer Centre in Guangzhou. Comments from Prof. Ming Cai, Dr. Da Yang, and Dr. Chundi Hu helped to improve the quality of the study.

REFERENCES

Adler, R. F., and Coauthors, 2003: The Version-2 Global Precipitation Climatology Project (GPCP) monthly precipitation analysis (1979–present). *J. Hydrometeor.*, **4**, 1147–1167, https://doi.org/10.1175/1525-7541(2003)004<1147:TVGPCP>2.0.CO;2.

Bergman, J. W., H. H. Hendon, and K. M. Weickmann, 2001: Intraseasonal air–sea interactions at the onset of El Niño. *J. Climate*, **14**, 1702–1719, https://doi.org/10.1175/1520-0442(2001)014<1702:IASIAT>2.0.CO;2.

Cai, M., 2003: Formation of the cold tongue and ENSO in the equatorial Pacific basin. *J. Climate*, **16**, 144–155, https://doi.org/10.1175/1520-0442(2003)016<0144:FOTCTA>2.0.CO;2.

Cai, W., A. Sullivan, and T. Cowan, 2011: Interactions of ENSO, the IOD, and the SAM in CMIP3 models. *J. Climate*, **24**, 1688–1704, https://doi.org/10.1175/2010JCLI3744.1.

Cane, M. A., S. E. Zebiak, and S. C. Dolan, 1986: Experimental forecasts of El Niño. *Nature*, **321**, 827–832, https://doi.org/10.1038/321827a0.

Carton, J. A., G. Chepurin, X. Cao, and B. Giese, 2000: A Simple Ocean Data Assimilation analysis of the global upper ocean 1950–95. Part I: Methodology. *J. Phys. Oceanogr.*, **30**, 294–309, https://doi.org/10.1175/1520-0485(2000)030<0294:ASODAA>2.0.CO;2.

Chang, C., Z. Wang, J. McBride, and C. Liu, 2005: Annual cycle of Southeast Asia—Maritime Continent rainfall and the asymmetric monsoon transition. *J. Climate*, **18**, 287–301, https://doi.org/10.1175/JCLI-3257.1.

de Boyer Montégut, C., G. Madec, A. S. Fischer, A. Lazar, and D. Iudicone, 2004: Mixed layer depth over the global ocean: An examination of profile data and a profile-based climatology. *J. Geophys. Res.*, **109**, C12003, https://doi.org/10.1029/2004JC002378.

Gill, A. E., 1980: Some simple solutions for heat-induced tropical circulation. *Quart. J. Roy. Meteor. Soc.*, **106**, 447–462, https://doi.org/10.1002/qj.49710644905.

Harrison, D. E., and G. A. Vecchi, 1997: Westerly wind events in the tropical Pacific, 1986–95. *J. Climate*, **10**, 3131–3156, https://doi.org/10.1175/1520-0442(1997)010<3131:WWEITT>2.0.CO;2.

Hong, C., H. Hsu, W. Tseng, M. Lee, C. Chow, and L. Jiang, 2017: Extratropical forcing triggered the 2015 Madden–Julian Oscillation–El Niño event. *Sci. Rep.*, **7**, 46692, https://doi.org/10.1038/srep46692.

Hurrell, J. W., and Coauthors, 2013: The Community Earth System Model: A framework for collaborative research. *Bull. Amer. Meteor. Soc.*, **94**, 1339–1360, https://doi.org/10.1175/BAMS-D-12-00121.1.

Kanamitsu, M., W. Ebisuzaki, J. Woollen, S. Yang, J. J. Hnilo, M. Fiorino, and G. L. Potter, 2002: NCEP–DOE AMIP-II

Reanalysis (R-2). *Bull. Amer. Meteor. Soc.*, **83**, 1631–1643, https://doi.org/10.1175/BAMS-83-11-1631.

Kao, H., and J. Yu, 2009: Contrasting eastern-Pacific and central-Pacific types of ENSO. *J. Climate*, **22**, 615–632, https://doi.org/10.1175/2008JCLI2309.1.

Kug, J.-S., and I.-S. Kang, 2006: Interactive feedback between ENSO and the Indian Ocean. *J. Climate*, **19**, 1784–1801, https://doi.org/10.1175/JCLI3660.1.

——, F. Jin, and S. An, 2009: Two types of El Niño Events: Cold tongue El Niño and warm pool El Niño. *J. Climate*, **22**, 1499–1515, https://doi.org/10.1175/2008JCLI2624.1.

Kumar, A., M. Chen, Y. Xue, and D. Behringer, 2015: An analysis of the temporal evolution of ENSO prediction skill in the context of the equatorial Pacific Ocean observing system. *Mon. Wea. Rev.*, **143**, 3204–3213, https://doi.org/10.1175/MWR-D-15-0035.1.

Latif, M., and Coauthors, 1998: A review of the predictability and prediction of ENSO. *J. Geophys. Res.*, **103**, 14 375–14 393, https://doi.org/10.1029/97JC03413.

Lau, K.-M., and S. Yang, 1996: Seasonal variation, abrupt transition, and intraseasonal variability associated with the Asian summer monsoon in the GLA GCM. *J. Climate*, **9**, 965–985, https://doi.org/10.1175/1520-0442(1996)009<0965:SVATAI>2.0.CO;2.

Lee, T., and M. J. McPhaden, 2010: Increasing intensity of El Niño in the central-equatorial Pacific. *Geophys. Res. Lett.*, **37**, L14603, https://doi.org/10.1029/2010GL044007.

——, and Coauthors, 2010: Record warming in the South Pacific and western Antarctica associated with the strong central-Pacific El Niño in 2009–10. *Geophys. Res. Lett.*, **37**, L19704, https://doi.org/10.1029/2010GL044865.

Lengaigne, M., E. Guilyardi, J. Boulanger, C. Menkes, P. Delecluse, P. Inness, J. Cole, and J. Slingo, 2004: Triggering of El Niño by westerly wind events in a coupled general circulation model. *Climate Dyn.*, **23**, 601–620, https://doi.org/10.1007/s00382-004-0457-2.

Lim, Y. K., R. M. Kovach, S. Pawson, and G. Vernieres, 2017: The 2015/16 El Niño event in context of the MERRA-2 reanalysis: A comparison of the tropical Pacific with 1982/83 and 1997/98. *J. Climate*, **30**, 4819–4842, https://doi.org/10.1175/JCLI-D-16-0800.1.

Lu, P., and J. P. McCreary, 1995: Influence of the ITCZ on the flow of thermocline water from the subtropical to the equatorial Pacific Ocean. *J. Phys. Oceanogr.*, **25**, 3076–3088, https://doi.org/10.1175/1520-0485(1995)025<3076:IOTIOT>2.0.CO;2.

MacMynowski, D. G., and E. Tziperman, 2008: Factors affecting ENSO's period. *J. Atmos. Sci.*, **65**, 1570–1586, https://doi.org/10.1175/2007JAS2520.1.

McGregor, S., A. Timmermann, F. Jin, and W. S. Kessler, 2016: Charging El Niño with off-equatorial westerly wind events. *Climate Dyn.*, **47**, 1111–1125, https://doi.org/10.1007/s00382-015-2891-8 .

McPhaden, M. J., 2012: A 21st century shift in the relationship between ENSO SST and warm water volume anomalies. *Geophys. Res. Lett.*, **39**, L09706, https://doi.org/10.1029/2012GL051826.

Menkes, C. E., M. Lengaigne, J. Vialard, M. Puy, P. Marchesiello, S. Cravatte, and G. Cambon, 2014: About the role of Westerly Wind Events in the possible development of an El Niño in 2014. *Geophys. Res. Lett.*, **41**, 6476–6483, https://doi.org/10.1002/2014GL061186.

Morss, R. E., and D. S. Battisti, 2004: Designing efficient observing networks for ENSO prediction. *J. Climate*, **17**, 3074–3089, https://doi.org/10.1175/1520-0442(2004)017<3074:DEONFE>2.0.CO;2.

Neelin, J. D., F. Jin, and H. Syu, 2000: Variations in ENSO phase locking. *J. Climate*, **13**, 2570–2590, https://doi.org/10.1175/1520-0442(2000)013<2570:VIEPL>2.0.CO;2.

Saji, N. H., and T. Yamagata, 2003: Possible impacts of Indian Ocean dipole mode events on global climate. *Climate Res.*, **25**, 151–169, https://doi.org/10.3354/cr025151.

Terray, P., S. Masson, C. Prodhomme, M. K. Roxy, and K. P. Sooraj, 2016: Impacts of Indian and Atlantic Oceans on ENSO in a comprehensive modeling framework. *Climate Dyn.*, **46**, 2507–2533, https://doi.org/10.1007/s00382-015-2715-x.

Tollefson, J., 2014: El Niño tests forecasters. *Nature*, **508**, 20–21, https://doi.org/10.1038/508020a.

Torrence, C., and P. J. Webster, 1998: The annual cycle of persistence in the El Niño/Southern Oscillation. *Quart. J. Roy. Meteor. Soc.*, **124**, 1985–2004, https://doi.org/10.1002/qj.49712455010.

Wang, X., W. Tan, and C. Wang, 2018: A new index for identifying different types of El Niño Modoki events. *Climate Dyn.*, **50**, 2753–2765, https://doi.org/10.1007/s00382-017-3769-8.

Webster, P. J., 1995: The annual cycle and the predictability of the tropical coupled ocean-atmosphere system. *Meteor. Atmos. Phys.*, **56**, 33–55, https://doi.org/10.1007/BF01022520.

——, and S. Yang, 1992: Monsoon and ENSO: Selectively interactive systems. *Quart. J. Roy. Meteor. Soc.*, **118**, 877–926, https://doi.org/10.1002/qj.49711850705.

Xie, P., and P. A. Arkin, 1997: Global precipitation: A 17-year monthly analysis based on gauge observations, satellite estimates, and numerical model outputs. *Bull. Amer. Meteor. Soc.*, **78**, 2539–2558, https://doi.org/10.1175/1520-0477(1997)078<2539:GPAYMA>2.0.CO;2.

Xu, J., and J. C. L. Chan, 2001: The role of the Asian–Australian monsoon system in the onset time of El Niño events. *J. Climate*, **14**, 418–433, https://doi.org/10.1175/1520-0442(2001)014<0418:TROTAA>2.0.CO;2.

Yu, J., F. Sun, and H. Kao, 2009: Contributions of Indian Ocean and monsoon biases to the excessive biennial ENSO in CCSM3. *J. Climate*, **22**, 1850–1858, https://doi.org/10.1175/2008JCLI2706.1.

——, H. Kao, and T. Lee, 2010: Subtropics-related interannual sea surface temperature variability in the central equatorial Pacific. *J. Climate*, **23**, 2869–2884, https://doi.org/10.1175/2010JCLI3171.1.

——, Y. Zou, S. T. Kim, and T. Lee, 2012: The changing impact of El Niño on US winter temperatures. *Geophys. Res. Lett.*, **39**, L15702, https://doi.org/10.1029/2012GL052483.

Zhang, C., 2005: Madden–Julian Oscillation. *Rev. Geophys.*, **43**, RG2003, https://doi.org/10.1029/2004RG000158.

Zheng, Y., R. Zhang, and M. A. Bourassa, 2014: Impact of East Asian winter and Australian summer monsoons on the enhanced surface westerlies over the western tropical Pacific Ocean preceding the El Niño onset. *J. Climate*, **27**, 1928–1944, https://doi.org/10.1175/JCLI-D-13-00369.1.